Fs-21 Peptides Can Form Both Single Helix and Helix−Turn−Helix

Wei Zhang, Hongxing Lei, Shibasish Chowdhury, and Yong Duan*

Department of Chemistry and Biochemistry and Center of Biomedical Research Excellence in Structural and Functional Genomics, University of Delaware, Newark, Delaware 19716

Received: December 2, 2003; In Final Form: February 28, 2004

Detailed folding processes and mechanisms of two alanine-based peptides (Fs-21 and MABA-Fs) were investigated by all atom molecular dynamic simulation with a new AMBER force field and Generalized Born continuum solvent model. Both peptides showed multiphase folding processes. Much like what has been envisaged by the folding funnel theory, the number of accessible conformations descended quickly as folding progresses. Interestingly, MABA-Fs and Fs-21 peptides exhibited notably different folding kinetics; the Fs-21-folding was a two-phase process while MABA-Fs went through three phases and folded more slowly than the Fs-21 peptide by four times. These difference highlights the contribution of the bulky N-terminal MABA group. Furthermore, it is found that helix−turn−helix conformation was the most stable state at 300 K, instead of the expected full helix conformation. At 273 K, however, the full helix became the most stable state. The turn structure was found to be stabilized mainly by the hydrophobic interactions. Statistical analysis of high-resolution PDB structures indicated that most helices are shorter than 16 amino acids. Taken together, we suggest that the intrinsic property of polypeptide chain dictates the formation of short helices in proteins.

Introduction

Helix is a common secondary structure in proteins. Its fundamental roles and relative simplicity make it a proper study template for both experimentalists and theorists. Structurally, α-helix is the simplest autonomous folding unit and often plays important roles in protein architecture. Theoretically, its formation has been the foundation of important models, including the diffusion-collision model[1−3] and framework model.[4,5] The classic helix−coil transition theory is yet another example, owing to the works of Baldwin, Scheraga, Schellman, Zimm, Bragg, Lifson, and Roig. The recent insurgence of interests in these simple peptides has been largely stimulated by several important advancements. Among which, the advent of experimental methods (e.g., the laser temperature-jump experiments pioneered by Gruebele and co-workers[6]) enabled experimental characterizations of the folding kinetics of these peptides and extended the studies to go beyond equilibrium measurements. The discovery that β-sheet dominated amyloid fibrils are the causative agents in a number of human diseases underscores the significance of a thorough understanding of the secondary structures, including α-helix, and their roles in protein stability.

Much like the classic helix−coil transition theory, the prevailing theory of helix formation has been based on the observation that it takes three consecutive residues to form the first turn and the first hydrogen bond of α-helix. Thus, formation of the first turn and the first hydrogen bond is entropically more difficult than formation of the subsequent portion of the helix and is therefore the likely candidate of the rate-limiting step. Our recent study on AK16, a alanine-based helical peptide, strongly suggested otherwise.[7] Instead, we observed that the rate-limiting step in helix formation is linked to unfolding of nonnative states. In the present study, we further examined the validity of our earlier findings and extended our studies to Fs-21 peptides.

* Corresponding author. Telephone: (302) 831-1099. Fax: (302) 831-6335. E-mail: yduan@udel.edu.

Because of its stability, the alanine-based peptide has been extensively used as the model peptides in studying the α-helix formation, both theoretically[7−11] and experimentally.[12−16] Most of the existing simulation studies have focused on the comparison with experimentally measured helicity and folding free energies. Despite the obvious poor cooperativity observed in most of the simulations, curiously, good agreement has been found between the measured and calculated folding enthalpies. These studies reaffirmed what has been proposed based on helix−coil transition theory. From a structural perspective, those analyses have been almost exclusively focused on the main-chain conformation, except our earlier study[7] and the work by Garcia[11] who studied the role of Arg side chains.

Fs-21 peptide is a 21-residue helical peptide (−AAAAA-$(AAARA)_3$A−) designed by Lockhart and Kim.[17,18] As this peptide unfolds over a relatively wide temperature range, Williams et al.[19] have studied its unfolding using a laser-induced temperature-jump method. The kinetics was monitored using time-resolved infrared (TRIR) spectroscopy. The experimental data were fitted with a double exponential kinetic model with first time constant less than instrumental limited 10 ns, and the second time constant (unfolding time constant) was 160 ± 60 ns. Thompson et al.[20] observed an ∼8-fold faster relaxation time (20 ns) for this peptide, the change of states were monitored by using the fluorescence of an N-terminal probe, 4-methylamino benzoic acid (MABA). A "kinetic zipper" model based on single-sequence approximation was used to explain the experimental results from which the helix growth rate was predicted $\sim 10^8$ s^{-1}. Lednev et al.[21] used UV resonance Raman spectroscopy (UVRS) to study the equilibrium conformation and the kinetics of thermal denaturation of the Fs-21 peptide. In this study, the protecting groups at the terminals were not included. The availability of rich experimental kinetic data provides an ideal test ground for theoretical models. Because these experiments are based on relatively small perturbations to equilibrated systems and are sensitive to the small changes in peptide

10.1021/jp037688x CCC: $27.50
Published on Web 05/07/2004

conformation, they not only compliment the existing equilibrium studies but also provide reliable ways to measure important quantities such as relaxation rates from which activation energies have been obtained. More importantly, the relaxation rates are based on relaxation signal and are relatively free from the errors introduced due to equilibrium calibration (discussed later).

Mutated Fs-21 has also been studied recently. Thompson et al.[22] have measured the kinetics of the helix−coil transition for the synthetic 21-residue peptide Ac-WAAAH(AAARA)$_3$A-NH$_2$, in which the Ala residues at positions 1 and 5 of Fs-21 were mutated to tryptophan and histidine, respectively. The side chain of tryptophan and histidine can interact when residues 1−5 form an α-helix. This allows the protonated histidine to quench the tryptophan fluorescence efficiently. The melting transitions measured by their *T*-jump fluorescence method were well-described by a single-exponential relaxation, with a rate of 3.3×10^6 s^{-1} (∼300 ns) at 301 K. The relaxation rate increased at higher temperatures. The estimated activation energy was ∼8 kcal/mol. A similar study has been done by Huang et al.[23] on a peptide containing D-Arg residue, Ac-YGG(KAAAA)$_3$-CO-D-Arg-CO-NH$_2$. Time-resolved infrared (IR) measurement following a laser-induced *T*-jump revealed biphasic (or multiphasic) relaxation kinetics. The slow relaxation constant, which was 140 ns at 300 K, gave an activation energy of ∼15.5 kcal/mol.

Garcia and co-workers[11] applied the replica exchange MD (REMD) method to study the effect of sequence variation on the formation of this Fs-21 peptide with explicit solvent model and compared with A21 (all alanine) peptide. They found that the side chain shielding effect of Arg helped to stabilize the helical segments. However, they did not provide kinetic information because of the methodological limitation. In this paper, we investigated the folding mechanism of both Fs-21 (Ac-AAAAA(AAARA)$_3$A-NH$_2$) peptide and the MABA-bonded Fs-21 (MABA-AAAAA(AAARA)$_3$A-NH$_2$) peptide (MABA-Fs) by all atom molecular dynamics simulations with the Generalized Born solvent model and compared this with experimental results. Our analysis showed that the most stable conformation changed with temperature. Interestingly, the helix−turn−helix conformation was the most stable state at 300 K.

Methods

MD Simulation. The AMBER simulation package[24] was used in both simulation and data processing. The peptides were represented by a recently developed force field.[25] The charges of the MABA group were obtained by RESP[26] fitting to the electrostatic potential calculated using Gaussian 98 with HF/6-31G*//HF-3-21G basis set. All simulations were started from fully extended conformation after energy minimization. A total of 25 trajectories were done for each peptide by assigning different initial random velocities. A Generalized Born (GB) model[27] was used for all simulations with an effective 0.2 M salt concentration (modeled based on Debye−Hückel theory). In the GB method, the solvent is treated as a high-dielectric continuum interacting with charges that are embedded in solute molecules of lower dielectric environment. No surface area term was used in the GB model. The interior and solvent dielectric constants were set to 1.0 and 78.5, respectively. The temperature was controlled at 300 K using a weak-coupling scheme.[28] SHAKE[29] was applied to constrain all bonds connecting hydrogen atoms and a time step of 2.0 fs was used to numerically solve the Newtonian equations. Each simulation was run for 100.0 ns to an aggregated simulation time of 2.5 μs for each peptide. The coordinates were saved at 10 ps intervals, and a total of 250 000 snapshots were produced for analysis.

The same procedure was used in the low-temperature simulations except that the temperature was kept at 273 K. Five trajectories were performed for each of the Fs-21 and MABA-Fs peptides. Since longer time is needed to reach equilibrium at lower temperatures, these simulations were extended to 200 ns.

Helical Content Analysis. Helical content was calculated based on both the main chain $\varphi-\psi$ torsion angles and the main-chain hydrogen bonds. In the torsion angle based approach, residues are defined as being helical when their $\varphi-\psi$ angles fall within the helical region ($\varphi = -57° \pm 30°$ and $\psi = -47° \pm 30°$). Main-chain hydrogen bonds were defined when the O−H distance is within 2.8 Å and the C═O−H angle is between 120° and 180°. Since one can study the main chain hydrogen bonds by monitoring the "1600−1670 cm^{-1}" band of amide hydrogen via FTIR, the helical content based on the main chain hydrogen bonds can be directly compared with experiments. Furthermore, because experimentally the 3_{10}, α-, and π-helix are indistinguishable in experiments, we counted all three species in our analysis. The helical contents averaged over all 25 trajectories (MABA-Fs, Fs-21) were fitted with weighted least-squares[7] to

$$H_t = H_\infty - \sum_i H_i \exp(-t/\tau_i) \qquad (1)$$

where τ_i and H_i are the relaxation time and helical content of *i*th phase, H_t is the helical content at time t and H_∞ is the expected helical content when the folding process reaches equilibrium.

The simulated snapshots were clustered based on a hierarchical method in which a snapshot was included into its closet cluster if the main-chain root-mean-square distance (RMSD) is smaller than 2.5 Å after sequential superimposition. The representative structures were compared, and the clusters whose representative structures were closer than 2.5 Å were merged together.[7]

Results

Differences between Fs-21 and MABA-Fs Peptides. The helical contents averaged over all 25 trajectories (MABA-Fs, Fs-21) are shown in Figure 1. Parts A and B of Figure 1 are the results based on $\varphi-\psi$ torsion angles. Fs-21 can be fitted nicely with eq 1 by a two-phase process, while three-phase transition was more appropriate for MABA-Fs. The calculated equilibrium helical content H_∞ was ∼54% for Fs-21 and ∼52% for MABA-Fs (Table 1), which agree very well with experimental measurements based on CD.[20]

The hydrogen bond results (Figure 1, parts C and D) reinforced the above conclusion about different phases. The estimated helical content was less than the $\varphi-\psi$-based result by ∼7% because H-bond method does not count the isolated residues. The fitting results of both approaches were summarized in Table 1.

The first phase was extremely fast. The relaxation times of this rapid phase were less than 0.05 and 0.1 ns for Fs-21 and MABA-Fs, respectively. As all the simulations started from fully extended states, the first step was the fast collapse caused by hydrophobic interactions. The average radius of gyration (R_γ) was reduced from over 14 to ∼8 Å within 0.1 ns, indicating a rapid packing collapse. More detailed discussions on R_γ are described in the latter part of this paper. At the end of the first phase, on average, more than one main-chain hydrogen bond

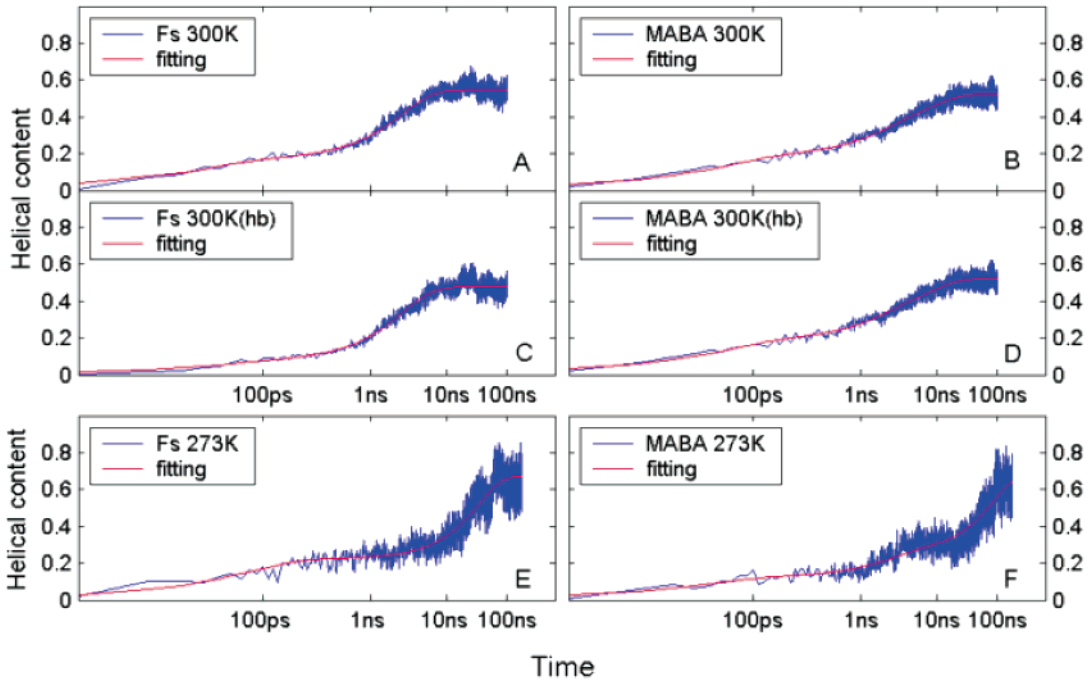

Figure 1. Average helical contents measured with different methods. The fitting results are based on eq 1 (see method). (A, B) 300 K results based on the torsion angle method. (C, D) 300 K results based on the hydrogen bonds method. (E, F) 273 K results based on the torsion angle method.

TABLE 1: Fitting Results of Relaxation Times and Helical Contents and Summary of Energetic Data

A. Fitting Results

	τ_1 (ns)	τ_2 (ns)	τ_3 (ns)	helical content (%)	ΔG_f (kcal/mol)	τ_f (ns)	τ_u (ns)
Fs-21							
Φ−Ψ, 300 K[a]	0.034	2.2		54.3	−0.10	4.0	4.8
Φ−Ψ, 273 K[c]	0.067	30.0		67.2	−0.43	45.5	90.9
H-bond, 300 K[b]	0.041	2.3		47.7	0.05	4.8	4.3
H-bond, 273 K[d]	0.110	30.0		60.2	−0.22	50.0	75.4
MABA-Fs							
Φ−Ψ, 300 K[a]	0.053	1.4	7.9	52.0%	−0.05	15.2	16.4
Φ−Ψ, 273 K[c]	0.039	2.0	80.0	67.6%	−0.44	118.3	250.0
H-bond, 300 K[b]	0.095	1.4	7.1	45.1%	0.12	15.6	13.0
H-bond, 273 K[d]		3.7	80.0	58.8%	−0.19	136.1	194.2

b. Summary of Energetic Data

	$E_{a,rel}$ (kcal/mol)	ΔH_f (kcal/mol)	ΔS_f (cal/K/mol)	$E_{a,f}$ (kcal/mol)	$E_{a,u}$ (kcal/mol)
Fs-21, Φ−Ψ	15.8	−3.3	−12.2	14.7	18.4
MABA-Fs, Φ−Ψ	14.0	−4.0	−14.4	12.4	16.4
Fs-21, H-bond	15.5	−3.1	−10.5	14.1	17.3
MABA-Fs, H-bond	14.6	−3.3	−11.4	13.1	16.3
exptl data					
Huang et al.	15.5	−7.8	−27.5	11.3	20.1
Thompson et al.	4.3−13.6[e]				
Lednev et al.	7.3−22.2[f]				

[a] 300 K fitting results according to helical content calculated with torsion angle method. [b] 300 K fitting results according to helical content calculated with main chain hydrogen bonds method. [c] 273K fitting results according to helical content calculated with torsion angle method. [d] Estimated energetic terms compared with experimental data. [e] Estimated based on the data in ref 22, although Thompson et al obtained $E_{a,rel}$ = 8 kcal/mol. The measured relaxation rates were $k_{rel} = 2.3 \times 10^6$ s^{-1}, 4.3×10^6 s^{-1}, 10×10^6 s^{-1}at T = 281K, 306K, 318K, respectively. Based on Arrhenius equation, $E_a = RT_1T_2/(T_1 - T_2)$ ln k_1/k_2. These three data points were grouped into three pairs and lead to $E_{a,rel}$ = 4.3, 13.6, and 7.2 kcal/mol, respectively. The average was $E_{a,rel}$ = 8.4 kcal/mol. [f] Estimated based on data in ref 21 and Lednev obtained an activation energy of 8±2 kcal/mol. The measured relaxation times were τ_{rel}= 180±60 ns, 120±50 ns, 70±30 ns at T = 310K, 321K, 337K, respectively. Our calculation took into account the uncertainty associated with each data point (e.g., τ_{rel}= 70±30 ns at T = 337K).

was formed and more than 3.6 residues were in the helical state. Thus, this rapid collapse process was accompanied by rapid initiation of short helices, consistent with what we observed in the AK16 peptide simulations.[7]

After the initiation phase, however, Fs-21 and MABA-Fs underwent different processes. Fs-21 reached its final state through one more phase with a relaxation time of ∼2.2 ns. Thus, Fs-21 folding was a simple two-phase process. In comparison, MABA-Fs underwent two more steps before it reached the equilibrium. The relaxation times of these two phases were, respectively, ∼1.5 ns and ∼7.1−7.9 ns. The final phase was an equilibrium stage at which the system reached a dynamic

equilibrium. The average helical content reflected those equilibrium results. The relaxation time of the last phase, which was the slowest step, was faster than the experimental folding time due to the continuum solvent model used in our simulations which neglects the solvent viscosity effect (discussed later).

However, the viscosity effect alone is insufficient to explain the qualitative differences between these two peptides. First, MABA-Fs peptide underwent three phases while Fs-21 only went through two. Second, Fs-21 folded with a rate of about 2 ns which is significantly faster than MABA-Fs peptide (7.1−7.9 ns). This suggests that the presence of MABA group at the N-terminal significantly changed the folding kinetics of MABA-Fs peptide. Apparently, the bulky MABA group can stabilize some of the nonnative states by presenting a large hydrophobic surface which facilitated formation and subsequently stabilized nonnative hydrophobic clusters. This then increased the number of folding steps from two to three. Because of the increased size of the hydrophobic cluster, unfolding of these clusters would be slower. This slowed the folding rates. This is consistent with our observations in other simulations. In the simulations of AK16, the folding was a three-phase process, much like MABA-Fs. However, a two-phase process was observed in a comparable set of simulations on AK14 in which AK14 folds with a significantly faster rate (data not shown). AK14 is shorter than AK16 by only two residues at the N-terminal (Try, Gly). The bulky ring structure and the potential hydrogen bond donor group (−OH, −NH, respectively) may be the main contributors to the slower folding rate and more folding phases in both cases.

CD results suggested that the helical content of MABA-Fs[20] is ∼50% at 300 K. This agreed very well with our result (∼52%). The calculated equilibrium helicity (Table 1) based on both torsion angle and hydrogen bonds showed that the helical contents of Fs-21 and MABA-Fs were similar (Fs-21 was ∼2% higher), consistent with the experimental observations that their "highest helical contents" were similar.[15,20] Thus, the MABA group appears to affect the equilibrium helical content only slightly (which may be attributable to the intrinsic helical propensity of the N-terminal MABA group). However, it changed the folding process from two phases to three phases and significantly reduced the folding rates.

Helix—Turn—Helix Is the Most Stable Conformation at 300 K. Experimental methods such as CD and fluorescence spectroscopy can provide accurate measurement on the equilibrium properties, such as helical content. However, the microscopic (conformational) information, which is crucial for the understanding protein folding, is difficult to obtain directly from experiments. To understand more about the folding mechanisms, clustering analysis of the simulation results was performed (see methods). The final numbers of clusters were 2350 and 2391 for Fs-21 and MABA-Fs, respectively.

According to the folding funnel theory,[30,31] there are numerous possible conformations at the beginning of folding. The possible conformations with local energy minima decrease to only a few when a protein approaches its folded state. These local minima may play important roles in affecting the folding rates. Proteins fold toward the native states through conformational search. Since each cluster is an ensemble of snapshots of similar structures, if we take each cluster as one possible conformation, we can qualitatively estimate the conformational search rate from the total number of clusters at different time periods. The rate, number of clusters per ns, measures how frequently the conformations were transformed at these stages. For the Fs-21 peptide, these rates were 223, 43, 20, and 18 for the time spans of 0−1, 1−10, 10−20, and 90−100 ns, respectively. For the MABA-Fs peptide, these rates were 248, 42, 21, and 18 for the same periods. This clearly demonstrated a descending trend of the rate of conformational changes as the folding progressed and was consistent with a funnel-like scenario. The results suggested that the helix−coil transition shares similar mechanisms with protein folding. However, this implies that the "nucleation and propagation" theory may describe just a small part of a complicated process. Furthermore, the 18 clusters/ns observed in the last 10 ns illustrated a dynamic equilibrium at final stage.

TABLE 2: Summary of Cluster Analysis at 300 K

	categories	0−1 ns	1−10 ns	10−20 ns	90−100 ns
Fs-21	full helix	0%	22.3%	30.5%	20.1%
	HTH	5.8%	21.1%	24.8%	41.6%
	AHTH	0%	5.4%	8.7%	1.2%
	GH	0%	3.2%	2.7%	3.9%
	helix tail	0%	0%	3.7%	2.8%
	HWH	2.0%	6.3%	4.2%	9.7%
	STH	10.1%	1.1%	0%	4.8%
	random coil	16.7%	3.0%	2.4%	0%
	populated clusters	13	14	15	12
	uncounted	63.7%	37.4%	23.0%	11.8%
	total clusters	248	375	211	182
MABA-Fs	full helix	0%	4.6%	13.1%	9.1%
	HTH	2.1%	23.1%	33.6%	30.3%
	AHTH	0%	7.6%	14.7%	12.7%
	GH	0%	0%	0%	6.4%
	helix tail	0%	3.2%	3.8%	3.8%
	HWH	0%	3.3%	6.3%	7.8%
	STH	22.9%	8.2%	7.6%	3.0%
	random coil	17.2%	0%	0%	0%
	populated clusters	14	16	22	19
	uncounted	57.8%	52.0%	20.9%	25.8%
	total clusters	223	385	197	177

Since poorly populated clusters do not represent the main features of the folding processes, we will focus our discussions on those most populated clusters. The results of clustering shown in Table 2 are the clusters with population larger than 1% (except 2% for 0−1 ns, because of the relatively high random distribution). These clusters were classified into eight categories (Table 2) according to their structure features and the representative structure of each category is shown in Figure 2. Among these, the structures of most categories can easily be discriminated except for the helix−turn−helix (HTH) and the adjusted helix−turn−helix (AHTH). The difference between HTH and AHTH is at the hydrophobic cluster between two helical parts. In the HTH, the two helix segments were antiparallel and a hydrophobic cluster was formed by contacts between the two segments. In AHTH, the hydrophobic cluster was either absent or only partially formed and the two helical segments were not antiparallel and were flexible. Those HTH clusters with ends bended were also assigned into the AHTH category.

According to the results shown in Table 2, the two most populated conformations were full helix and HTH. Since the folding mechanisms are different between Fs-21 and MABA-Fs, their clustering results are discussed separately.

For Fs-21, an interesting observation was that the HTH became more populated than the full helix as folding progresses. About 20% of the snapshots were in full helix conformation after the first ns which increased to its highest value (∼30%) during 10−20 ns and decreased to ∼20% at the last 10 ns. In comparison, the HTH started to appear at the initial step (within 1.0 ns) and its population increased with time and reached ∼41% within the last 10 ns, more than twice as much of the full helix. In fact, the HTH conformation was the most-populated category, suggesting it is the "native state" under the simulation conditions. This is a little surprising because it is generally expected,

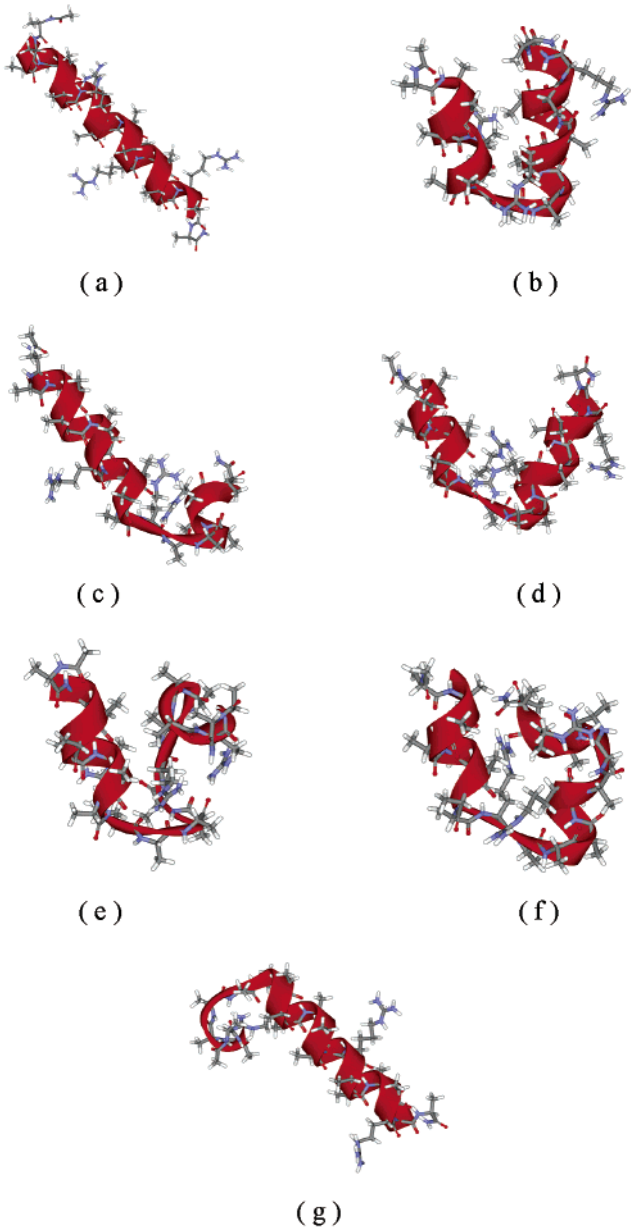

Figure 2. Representative structures of different categories: (a) full helix, (b) helix−turn−helix (HTH); (c, d) adjusted helix−turn−helix (AHTH), (e) helix−wind−helix (HWH), (f) globular helix (GH), (g) helix tail. Single turn helix (STH) and random coil used the regular definition; they do not have representative structures.

according to the helix−coil transition theory, that the native state would be the full helix.

A similar trend was observed in the MABA-Fs simulations in which the HTH conformation remained more populated than the full helix throughout the simulations. Population of HTH reached more than 30% during the last 10 ns and that of full helix was only less than 10% for the same period. The reduced population of full helix was due to the N-terminal hydrophobic MABA group that has the tendency to form clusters with alanines and stabilizes the compact structures. This also explains the slight reduction of helicity observed in MABA-Fs peptide in comparison to Fs-21 peptide. Nevertheless, our simulations suggested that the HTH could be the native state of Fs-21 peptides.

On the other hand, the populated clusters of MABA-Fs were more widely distributed than Fs-21. There were still more populated clusters (>1%) for MABA-Fs than Fs-21 after reached the equilibrium stage. Thus, the presence of MABA group enhanced the heterogeneity of the structures at equilibrium.

Radius of Gyration. Although our earlier cluster-based analysis suggested that the HTH conformation could be the native state of Fs-21 peptides, a possible counterargument is that the full helix included only a few clusters, while HTH consisted of more clusters. Since the clustering method was based on the main-chain rmsd, as long as the backbone stays straight, even when both ends were flexible, the conformation should still be classified into full helix. Other possible full-helix conformations include somewhat bent but otherwise well-formed helices. In addition, different states of protein folding are conformation ensembles instead of one certain structure. Therefore, further analyses were performed based on radius of gyration (R_γ) and main-chain hydrogen bonds.

Radius of gyration measures the compactness of polymers. Chain collapse is considered one important step in protein and peptide folding. The upper limit of chain collapse rate can be used to estimate the maximum folding rate of given protein in absence of an energy barrier.[32] In our case, because of the extended conformation of the full helix, radius of gyration can also provide useful information on the folding kinetics.

Figure 3 shows the average radius of gyration over 25 trajectories. Both MABA-Fs and Fs-21 showed the similar trends. First, the peptides collapsed rapidly to the most compact conformations within 1.0 ns. The insets of Figure 3 show the details within the first 500 ps. Three steps can be observed. The first step was very fast in which R_γ decreased from 14 to less than 10 Å within 20 ps. This was due to the fact that the simulations started from straight-chain conformation which was an unfavorable state both entropically and enthalpically. In the second step, R_γ decreased by ~ 1 Å over about 30 ps. The last step was much slower and R_γ decreased by ~1 Å in about 500 ps. Compared with the helix initiation time (~0.05−0.1 ns), the collapse occurred concomitantly with helix initiation. This corresponded to the initial hydrophobic collapse process. This is interesting because, while hydrophobic collapse has been viewed as an important step in protein folding, it has been very much ignored in the studies of helix−coil transitions using alanine-based peptides until recently.[7]

The radius of gyration then relaxed gradually with increasing flexibility. After about 20 ns, R_γ reached a peak (~ 9Å) and then decreased gradually with an even higher degree of flexibility. This can be attributed to the transitions between full helix and HTH since R_γ of full helix and HTH were ~10.1 and ~7.2 Å, respectively. The increase of full helix conformations was the reason for the R_γ increasing after the initial compact stage. The R_γ decreased when full helix was transformed to thermodynamically more stable HTH conformations. This reinforced the earlier conclusion that the full helix was not the native state.

Figure 4 further shows the radius of gyration in several typical single trajectories. A striking feature was that the R_γ was bimodular and fluctuated between the full-helix (~10 Å) and the helix−turn−helix (~7 Å) conformations. For Fs-21, these two states were relatively stable. For MABA-Fs, an intermediate R_γ was also observed.

Two-dimensional histograms were calculated from the saved snapshots for R_γ and the number of main chain hydrogen bonds. The potential of mean force is shown in Figure 6 as 2-D contour maps. Both MABA-Fs and Fs-21 peptides exhibited similar free energy surfaces. At 300 K, both showed that the most stable

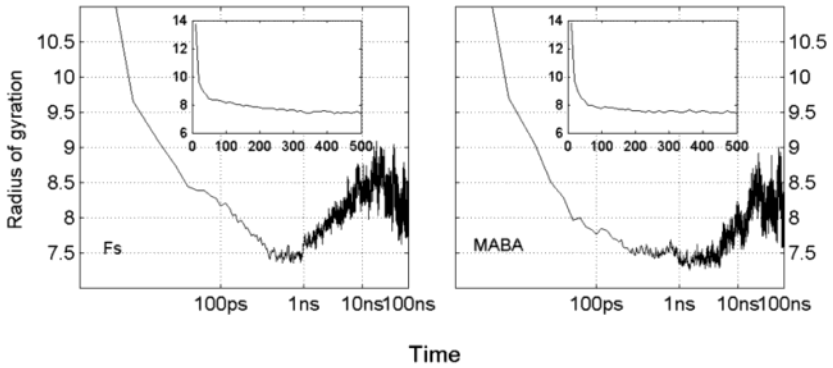

Figure 3. Average radius of gyration of the total 25 trajectories at 300 K. The insets show the variation of average radius of gyration within the first 500 ps. Vertical axes are in Angstroms.

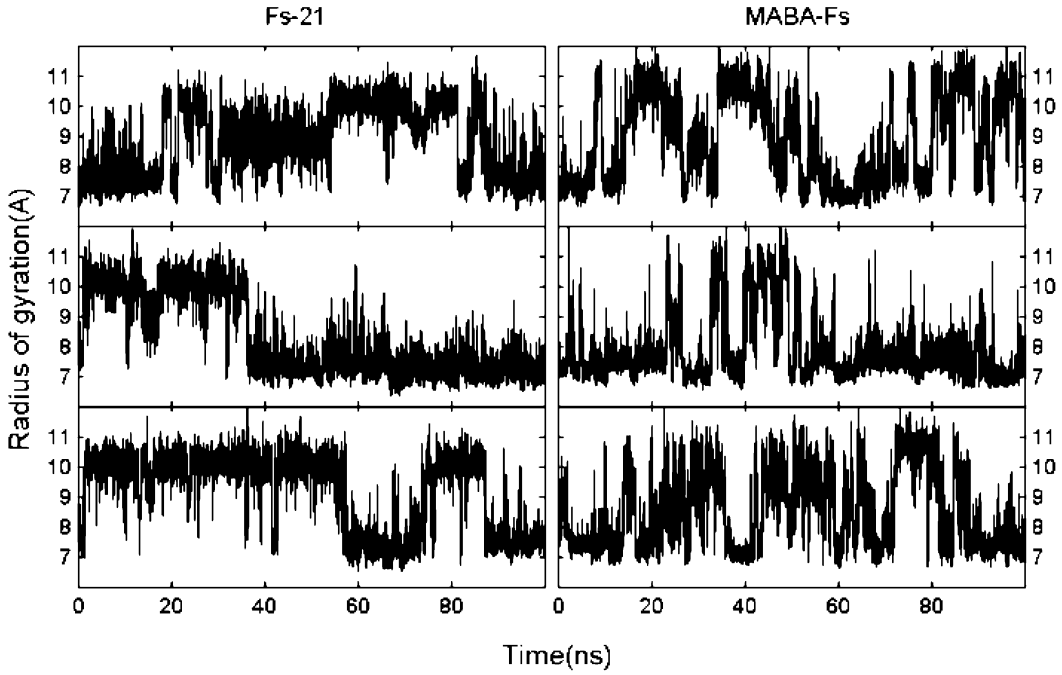

Figure 4. Radius of gyration of single trajectory. Three typical trajectories of both Fs-21 and MABA-Fs are shown. (R_γ of full helix: ~10.1Å, R_γ of HTH: ~7.2Å.)

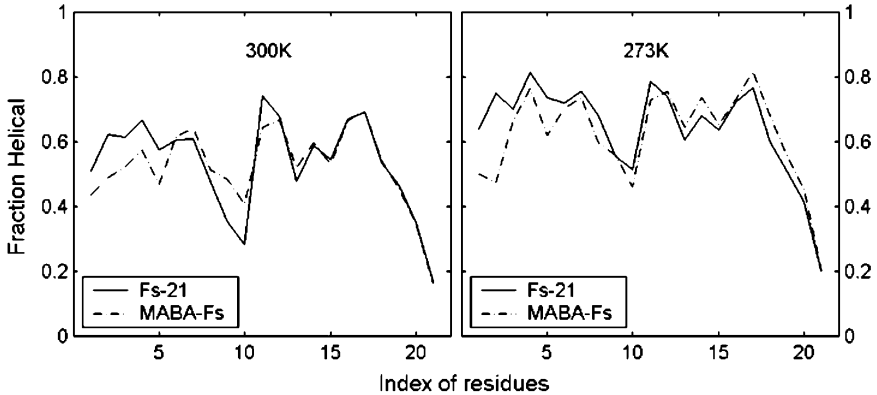

Figure 5. Fractional helicity of residues at different positions. The residue indices exclude the N-terminal protecting groups. The fractional helicity was calculated from the last 50 ns of the trajectories.

state was at $R_\gamma = \sim 7.5$ Å with about eight main chain hydrogen bonds. This was the HTH state described earlier. Comparatively, the full helix state, $R_\gamma = \sim 10$ Å with ~14 main chain hydrogen bonds, was about 0.5 kcal/mol less stable. This further corroborates our earlier conclusion based on clustering analysis.

Identical low energy conformers were observed at both temperatures: the one with less main-chain hydrogen bonds and smaller R_γ was the HTH; the other with more hydrogen bonds and larger R_γ was the extended helix. The R_γ and number of hydrogen bonds agreed well with the representative HTH and full helix conformations. The HTH conformation was more stable at 300 K for both Fs-21 and MABA-Fs, with ~1.0 kcal/mol lower energy than the extended helix. At 273 K, the two conformations had similar free energies in MABA-Fs, while

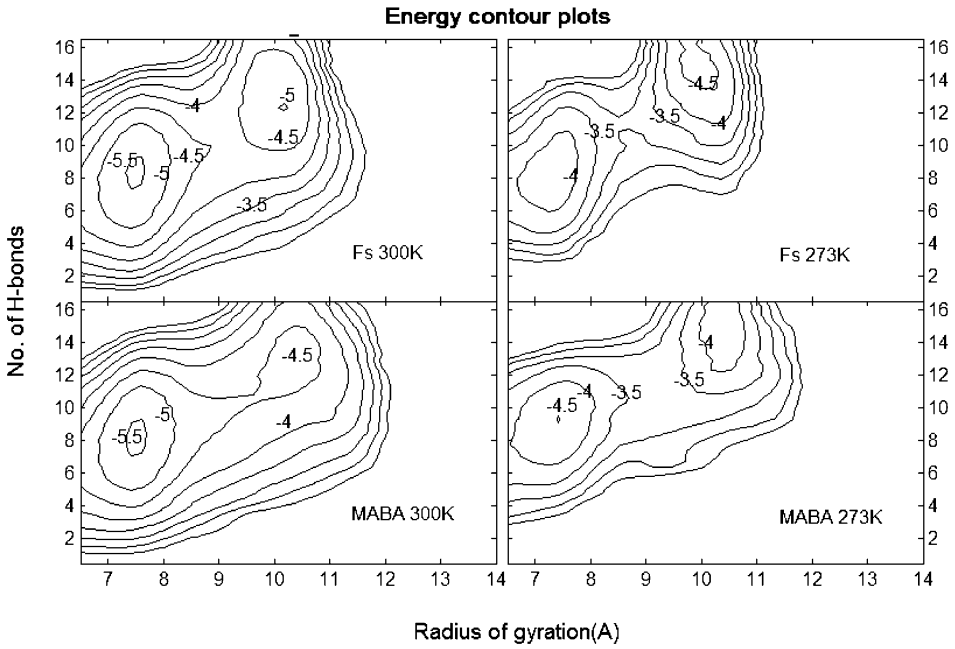

Figure 6. Contour plot of the potential of mean force as a function of total number of hydrogen bonds and radius of gyration based on the last 50 ns data. Contour levels are drawn at 0.5 kcal/mol intervals, and the lowest isoenergetic lines are marked.

the extended helix became more stable than HTH by ~0.5 kcal/mol for Fs-21.

Hydrophobic Interactions Stabilize Turn Conformation. It has been discussed that hydrophobic interaction plays important roles in protein folding. Other forces such as hydrogen bonding and electrostatic interaction may also affect protein stability.[33] We also observed that breaking nonnative hydrophobic clusters was the rate-limiting step in the folding of AK16 peptide.[7] Analysis of the structures of those most populated or most stable clusters may help to describe the roles of different forces in the studies peptides.

The native HTH structures showed very well compact conformations. Between the two helix arms, the hydrophobic side chains faced each other forming a strong hydrophobic core. On the top of the core, methane group of two end residues (Ala_2 and Ala_{21}) formed a close contact. In the middle part were the methane groups of Ala_6 and Ala_{17}. An interesting observation was that the bottom part, which was near the turn region, was formed by the side chains of Arg_9 and Arg_{14}. The two Arg side chains were antiparallel with each other and their aliphatic groups (from C_α to C_δ) were close to each other (3.7−6.2 Å) and formed the bottom part of the hydrophobic core. The polar guanidinum groups of the side chains pointed outside of the core into the solvent. The plane guanidinum group of Arg_{14} was nicely embedded between the end of N-terminal helix and the turn region. The interaction between the main chain carbonyl groups and the guanidinum group of Arg_{14} may also stabilize such conformation. Therefore, the turn region was stabilized by three factors: the hydrophobic interaction, the electrostatic interaction, and the steric effect of the guanidinum group.

Another interesting observation was that the turn structure was kept in all populated conformations except the full helix. The hydrophobic interactions between the methane groups were frequently broken, because of the flexibility of the end groups, while the one formed with Arg_{14} was always there. Even sometimes when the other Arg side chain flapped away, it will retain the hydrophobic interaction with the methane group of Ala at the opposite helix arm. Since the hydrophobic stem of Arg_{14} side chain played such an important role in stabilizing turn conformation, a similar effect was expected at Arg in other positions. In fact, we did observe such similarities. One example was the helix−wind−helix conformation (Figure 2e) which is one of the most populated clusters. It had the same N-terminal helix segment and the middle turn region structure as HTH, but the C-terminal helical segment bent and broken to a shorter helix, a second turn was formed which was stabilized by same factors as the middle turn except by Arg_{19}. Those results suggested that for amino acids with long side chains, such as Arg, the hydrophobic interactions formed with the aliphatic side chain stems may play stabilizing roles.

Helicity of Individual Residues. Figure 5 shows the average helicity per residue of the peptides based on the simulation results of last 50 ns. The only significant difference between MABA-Fs and Fs-21 was that the N-terminus of MABA had a lower helicity because of the bulk MABA group. For both peptides, the C-terminus showed higher flexibility and lower helicity which is consistent with what we observed in cluster analysis: most bend and helix breaking occurred at C-terminal. The middle turn region (residues 9 and 10) showed notably lower helicity whereas residues 3−8 and 11−18 were the two relative high helicity segments, which was consistent with the highly populated HTH conformations.

Garcia et al.[11] studied the Fs-21 peptide with explicit solvent model. They found the carbonyl groups had the lowest water coordinating number when the amino acid was four residues before Arg. They explained that was because the Arg side chain shielded the carbonyl oxygen atom from exposure to water. They also observed the higher helicity of the amino acids' two residues before Arg and concluded that the shielding effect was caused by the favorable interaction of charged side chain with carbonyl oxygen that stabilized the helix. The similar observation was made in our results (Figure 5). The residues that were two and three amino acids before Arg (residues 6, 7, 11, 12, 16, 17) had the highest helicity. However, the residues that were four amino acids before Arg (with the lowest water coordination number in Garcia's results) showed locally the lowest helicity (residues 5, 10, 15). The low helicity at around residue 10 (the turn region in our simulations) was also observed in Garcia's

TABLE 3: Summary of Cluster Analysis at 273 K

		analysis (%)						
	categories	0−1 ns	1−10 ns	10−20 ns	20−50 ns	50−100 ns	100−150 ns	150−200 ns
Fs-21	full helix	0%	0%	0%	26.4%	55.3%	46.5%	52.3%
	HTH	0%	0%	0%	4.%4	8.3%	17.7%	18.2%
	AHTH	0%	27.4%	16.6%	16.7%	13.9%	8.1%	0%
	GH	0%	0%	0%	0%	0%	5.7%	4.3%
	helix tail	0%	0%	7.1%	5.4%	7.5%	3.8%	0%
	HWH	0%	6.3%	0%	0%	0%	9.7%	18.5%
	STH	54.0%	17.4%	31.4%	12.9%	1.1%	2.3%	0%
	random coil	35.6%	40.4%	8.1%	6.6%	0%	0%	0%
	others	0%	0%	19.8%	19.8%	6.0%	1.1%	0%
	no. of populated clusters	9	11	12	14	14	11	7
	uncounted	10.4%	8.5%	15.0%	7.8%	7.9%	5.1%	6.7%
MABA-Fs	full helix	0%	12.8%	10.6%	14.2%	24.5%	34.2%	34.9%
	HTH	0%	0%	8.1%	6.9%	19.4%	30.4%	38.9%
	AHTH	0%	0%	0%	16.2%	5.7%	20.7%	10.3%
	GH	0%	0%	0%	0%	0%	0%	0%
	helix tail	0%	1.5%	0%	1.0%	14.5%	9.1%	3.4%
	HWH	0%	0%	7.1%	0%	1.4%	0%	6.4%
	STH	18.8%	25.0%	5.1%	2.6%	8.2%	0%	0%
	random coil	65.4%	39.2%	58.0%	47.3%	13.8%	0%	0%
	others	10.2%	2.0%	4.6%	3.6%	1.1%	0%	0%
	no. of populated clusters	8	8	10	14	17	12	9
	uncounted	5.6%	19.5%	6.5%	8.2%	11.4%	5.6%	6.1%

explicit solvent simulations.[11] Taken together, our observed helicity distribution along the peptide agreed remarkably well with what was found in the explicit solvent simulations by Garcia et al. [11]

Temperature effect (Simulation at 273 K). Although folding of Fs-peptide (and its derivatives) has been proposed to be two-state, the transition between the (presumably) denatured state at high temperature and the native state at low temperature is notably smoother than that for typical small globular proteins. While this smoothness might be attributable to a number of underlying physical mechanisms, the variation provides an ideal case for quantitative comparison on the energetics (i.e., folding enthalpy and entropy).

The helical content analysis (Table 1) showed that the temperature change did not alter the folding processes, albeit that, as expected, the equilibrium helicities were notably increased and the rates were significantly reduced at the low temperature. There were 2-folding phases for Fs-21 and three phases for MABA-Fs at 273 K that were also the cases at 300 K. The calculated 67−68% equilibrium helical contents for Fs-21 and MABA-Fs further demonstrated that MABA group had little effect on the equilibrium helical content. The low-temperature had minimal effect on the collapse phase which still finished within 100 ps. The most significant difference was that the folding rates of both peptides were more than 10 times slower than 300 K in both peptides, suggesting a significant enthalpic contribution to the activation barrier. One can estimate that the activation energies were 15.8 kcal/mol for Fs-21 and 14.0 kcal/mol for MABA-Fs peptide.

The same set of the most populated clusters was found at 273 K rather than at 300 K (Table 3), albeit with different distributions. A notable change, in comparison to 300 K, was the increase in population of full helix and HTH, the two clusters with highest helical content. At 273 K, these two types of clusters represented more than 70% of the total population during the final stages (last 50 ns) which was significantly higher than the 39% for MABA-Fs and 61% for Fs-21 at 300 K. The increase in population accounted for the main contribution to the helicity increase. Another notable change was that the full helix population notably increased in respect to the population in the HTH. In fact, for Fs-21, full helix became the most populated cluster at 273 K and was three times more favorable than HTH. In the case of MABA-Fs, population in the full helix conformation also increased by more than three times compared with 300 K. This is clearly demonstrated in Figure 6. At 273 K, the most favorable region on the 2-D potential of mean force (PMF) contour map of Fs-21 is now located at around $R_\gamma = 10$ Å with ∼14 hydrogen bonds, corresponding to the full helix conformation. For MABA-Fs peptide, although the most favorable region was still at $R_\gamma = \sim 7.5$ Å with ∼8 hydrogen bonds, the HTH region, the difference between full helix and HTH was substantially reduced.

In terms of helicity of individual residues, there was an overall increase across all residues at lower temperature (Figure 5). However, the relative helicity per residue remained almost the same as 300 K. The turn region (residues 9 and 10) still exhibited reduced helicity because of the existence of HTH conformations, although the difference at 273 K is less profound than that at 300 K due to the increased population in full helix conformation.

Discussions

Helix−coil transition has been one of the very well-studied subjects. There are large amount of equilibrium and kinetic data. Thus, critical comparisons can be made that can shed light on the accuracy of the simulations. In the past, comparisons were mostly based on equilibrium measurement that requires careful calibration of the reference states (both full helical and unfolded states). For quantitative studies, errors in these reference states can become an important source of uncertainty. The elegant experiments by Lednev et al.[21] are good examples of this type of calibration. In their work, the full-helical state was assumed to be a helix in helix-enhancing medium, TFE (45% v/v), and at low temperature (−4.0 °C). Because of such an elaborate calibration, they found that the Fs-21 peptide had a substantially lower helicity than what was found from earlier studies that were not carefully calibrated. In fact, they found only about 60% helicity at around −4 °C which is close to the 67% helicity at 0°C found in our simulations. The difference may be attributable to the way that Lednev et al.[21] calibrated the coiled state which might have underestimated the helicity (discussed below).

While calibration of the full-helical state can be achieved, it is also important to obtain reliable measurements on the helicity at the fully denatured state. Traditionally, this has been done based on circular dichorism signal. Lednev et al argued, however, that short helical peptides are disordered and therefore should have 0% helicity (0−40°C). On the basis of this calibration, they concluded that the Fs-21 peptide was disordered and had 0% helicity at 75 °C. This further lead to an activation energy of folding of about −4 kcal/mol, which was anti-Arrhenius and disagreed with the majority of existing experimental data done by others (e.g., Huang et al.[23] obtained 11.3 kcal/mol refolding activation energy). Although such behavior could due to the failure of two-state assumption, the calibration procedure might also have played a role which had a tendency to significantly underestimate the helicity.

Fortunately, kinetic data based on rapid *T*-jump experiments is relatively free from the uncertainty associated with calibration of helicity at either the full-helical state or the fully denatured state. These experiments are particularly appealing not only because they can measure the kinetic rates to extremely short time scales but also they are rather independent of detailed definition of helical content because they measure the relaxation process immediately after the rapid temperature jump. In these experiments, the change of population among the states is measured and the rates of relaxation are obtained reliably. This is clearly exhibited in Table 1b in which the available experimental data all suggested consistent activation energies of relaxation, $E_{a,rel}$, to be around 14−16 kcal/mol, not withstanding the differences among the peptides and monitoring methods used in the experiments. The large variation is largely due to the uncertainty and the accuracy in experiments.

We have estimated the $E_{a,rel}$ based on simulations at both 273 and 300 K and summarized the results in Table 1b. For Fs-21, an activation energy of 15.5−15.8 kcal/mol was obtained which agrees well with Huang et al.[23] For MABA-Fs peptide, we obtained an activation energy of 14.0−14.6 kcal/mol, which also agrees qualitatively with the results of Thompson et al.[22] These encouraging agreements highlight the accuracy of the simulations.

We also calculated the equilibrium properties, including folding enthalpy and entropy, from which we estimated the activation energies of folding and unfolding. One caveat of this type of calculations, as we noted above, is that they are very sensitive to the definition of both fully folded (helical) state and the fully unfolded coiled state. Nevertheless, based on the van't Hoff equation, our estimated $\Delta H_f = -3.1$ to -3.3 kcal/mol and $\Delta S_f = -10.5$ to -12.2 (cal/mol)/K of Fs-21 and $\Delta H_f = -3.3$ to -4.0 kcal/mol and $\Delta S_f = -11.4$ to -14.4 (cal/mol)/K for MABA-Fs peptide. These results were significantly lower than experimentally derived helix formation enthalpy (∼0.9−1.5 kcal/mol residue)[13,16,34]. This discrepancy, as we discussed earlier, could be due to the uncertainty associated with the calibration procedure used in many experiments.

By assuming small peptide to have zero helicity and using their CD spectrum for calibration, one runs into the risk of artificially shifting the equilibrium toward the coiled state. For example, when one uses $\theta(\lambda = 222\ \text{nm})_r = -2340$ (deg cm^2)/dmol, which is typically used in other studies instead of $\theta(\lambda = 222\ \text{nm})_r = -3200$ (deg cm^2)/dmol, one may obtain a folding enthalpy of about −7 to −9 kcal/mol, which would be close to the value obtained by others on comparable peptides.[23] However, it would be substantially smaller than the one obtained by Lednev et al.[21] (−12 kcal/mol). This exercise illustrates the sensitivity of the calibration. The associated uncertainty could be exacerbated when the calculations were based on the measurements at the regime close to either fully unfolded or fully folded conditions. Furthermore, because CD is more sensitive to long helices, the existence of short and transient helices may be difficult to detect on the basis of the CD signal alone. For example, Lednev et al.[21] found that Fs peptide can be 0.31 helical when measured by Raman spectrum which is more than twice as much as that observed by CD (0.14). Clearly, this level of discrepancy could add to the uncertainty. Interestingly, if one uses 0.31 to calibrate, the folding enthalpy would have been −6.5 to −7.3 kcal/mol.

Another possible source of error could be the underlying force field parameters and the Generalized-Born continuum solvent model. If we use −7 kcal/mol as the basis for comparison, our simulation underestimated the folding enthalpy by about 3 kcal/mol or less than 0.2 (kcal/mol)/residue. Such a small error requires a fine-tuning of the simulation parameters and is beyond the scope of the present study. Notwithstanding this error, our calculated activation energies agreed with experiments very well. The calculated activation enthalpy of folding ranged from 12.4 to 14.7 kcal/mol (or 0.59 to 0.7 (kcal/mol)/residue). This is comparable to the 0.59 (kcal/mol)/residue of Huang et al.[23] suggesting that the simulations captured the main characteristics of the folding process.

It has been believed that formation of isolated helices is a two-state process. Evidence of such simple kinetics included a simple exponential relaxation process and satisfactory fitting of helicity based on the van't Hoff equation. Recently this view has started to change, largely due to the increasing access to the short time events. Huang et al. observed a biphasic process on a small α-helical peptide.[23] The fast-phase was observed at relatively low temperature when the kinetic rate of the slower phase differed significantly from that of the fast-phase. In our simulation, we also observed a biphasic process for the Fs-21 peptide while the folding of MABA-Fs peptide appears to involve three phases.

Because of the short-time nature, it is difficult to characterize the fast-phase in experiments. In our simulation, the fast-phase was associated with the initiation of the transient short helices as envisaged by the diffusion-collision model. In this phase, the peptides underwent rapid collapse driven by the hydrophobic force and formed primarily random coils with partial helical structures. In the slower phase, the peptides overcame the nonnative states and reached a dynamic equilibrium. The intermediate phase of MABA-Fs was caused by the bulky MABA group which stabilized some of the nonnative states.

An HTH conformation such as helix−hairpin is a common motif in proteins. In our previous study on AK16 peptides, HTH was found to be transient and was a transition state.[7] Recently, Cui et al. reported a folding pathway study of an 18-residue peptide E6ap with helical NMR structure, and found the existence of a metastable state that resembles the HTH conformation.[35] Hoffmann and Knapp[36] studied a 26 residues HTH protein with simplified lattice model and observed a diffusion-collision folding behavior. In the present study, we observed that alanine-based peptides may form HTH as the most stable conformation at room temperature. On the basis of replica exchange simulations, Nymeyer and Garcia [37] suggested that the HTH structures in Fs peptide were artificially stabilized by the Generalized Born/surface area (GB/SA) model when compared with explicit solvent. However, their explicit solvent simulations clearly showed that the helicity of Fs-21 peptide was notably lower at the middle portion. In our opinion, this was indicative of helix unwinding at the middle of the peptide,

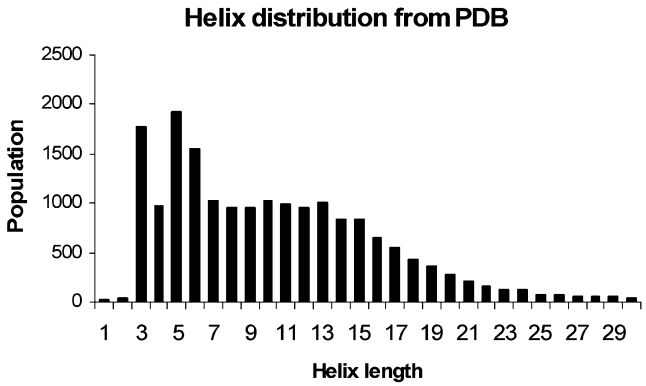

Figure 7. Distribution of different length α-helical segments based on Protein Data Bank (PDB) X-ray structures. A total of 2150 nonhomologous protein chains were obtained from PDB that have less than 30% sequence homology and better than 2.0 Å resolution.

which would be in qualitative agreement with our results. Nevertheless, experiments, such as small-angle X-ray scattering, can effectively differentiate these two types of conformations (i.e., HTH and single helix) since the size of HTH is considerably smaller than the single helix. These experiments should indicate a reduction in the average size when temperature is raised from 273 K to room temperature. The average size should again increase at high-temperature regime when the peptides start to become random coils.

To examine our conclusions further, we sampled 2150 nonhomologous protein chains from the Protein Data Bank (PDB) using the method developed by Wang and Dunbrack.[38] These chains have less than 30% sequence homology and better than 2.0 Å resolution. A total of 11 800 helix segments were found in these protein chains. Figure 7 shows the statistical distribution of helix lengths. Except the short helices of less than six residues, there are about the same number of helices that are 7−14 residues long. However, the population decreases sharply with increasing helix length after 15 residues. For example, on average there are about 1000 helices that are 7−14 residues. There are only less than 500 helices that are 18-residues long. A similar distribution has been observed in the statistical analysis results of PDB structures by others.[39] These results reinforce the conclusion that the stability of helix depend on the lengths. Interestingly, in comparison to our earlier study in which we observed that the full-helical conformation was the most stable state of a 16-residue peptide (AK16), the most populated state of the 21-residue peptide is not the full-helical structure at 300 K. However, at a lower temperature (273 K), the full-helical conformation became the most populated state, as evidenced by the PMF plot (Figure 6) based on the last 50 ns data for both 273 and 300 K.

Formation of helices depends on several factors, including the local helix propensity of the sequence, interactions of neighboring side chains, and interaction with solvent. The latter is particularly important for small peptides because they are expected to be almost fully exposed to solvent. Traditionally, hydrogen bonds were considered an important factor. Indeed, when one only considers peptides in the gas phase, hydrogen bonds are the most important and are likely the dominant factors. For a peptide in aqueous solution, however, the contribution of hydrogen bonds diminishes substantially. This has been eloquently discussed recently by Baldwin[40] and has been well-recognized in the protein-folding community. Thus, the focus on the main-chain hydrogen bond is somewhat contradictory to the general understanding of peptides in solution. Therefore, in our analyses, hydrogen bonds and helicity were treated as an "order parameter" and further analyses were focused on structural characterization (rather than simple counting of hydrogen bonds). This departure from the traditional hydrogen-bond-centric theory has significantly broadened our scope. So much so, we found rather dynamic folding process. In fact, the folding behavior of these small peptides showed qualitatively similar process as those of small proteins. For example, the initial step was a coupled process in which short helices initiated during the hydrophobic collapse. Subsequently, we also found, depending on the simulation temperature, that HTH can be a well-populated species.

Among the factors stabilizing the HTH conformation, the hydrophobic contacts across the two helical segments account for the contributions from interactions with solvent. The fact that the single-helix is the most stable conformation at low temperature (0 °C) suggests that HTH is also entropically more favorable which is not surprising. With the increasing temperature, one would expect that the hydrogen bonds that were partially responsible for holding the helix together would be weakened. This, coupled with the hydrophobic force, drove the peptide toward the HTH conformation.

For a peptide of 21 residues, one would expect a full-helical conformer to have maximum of 17 hydrogen bonds. The full-helical conformation described above corresponds to the conformation in which there are about 14 hydrogen bonds, as shown in Figure 6. The reduced number of hydrogen bonds reflects the fact that the terminal residues cannot form hydrogen bonds and are mobile. On the other hand, experimentally one often finds as many as four to seven terminal residues in the random coil state. Thus, our results are qualitatively consistent with other experiments.

The lack of representation of solvent viscosity can be a significant source of error for the calculations of folding rates.[41] Thus, it is not surprising that they differ significantly from existing experimental data.[19−22] Our calculated folding rates can only serve as indicators of relative folding rates. Despite this, the excellent agreement between our calculated and experimental activation energies demonstrates that our simulations captured the main characteristics of the folding processes of these peptides.

Conclusion

Detailed folding processes and mechanisms of Fs-21 and MABA-Fs were investigated by all atom molecular dynamic simulations. Multiphase folding processes were observed for both peptides. The bulky N-terminal MABA group was responsible for the different folding processes and different folding rates (∼2 and ∼7 ns, respectively). The helix−turn−helix conformation was found to be the most populated state at 300 K, which was about 1.0 kcal/mol more stable than the full helix conformation. Temperature change affected the relative stability of different ensembles and the full helix became more stable (∼0.5 kcal/mol lower than HTH) at low temperature (273 K). The turn structure was found to be stabilized mainly by hydrophobic interactions.

Acknowledgment. Helpful discussions with Prof. Robert Baldwin, Mr. Matthew Lee, and other members in Y.D.'s group are gratefully acknowledged. This work has been supported by research grants from NIH (RR15588, PI Lenhoff, GM64458 and GM67168 to Y.D.), the state of Delaware, University of Delaware, University of Delaware Research Fund, and Delaware Biotech Institute (to Y.D.). Usage of VMD, UCSF Midas, and WebLab viewer graphics packages are gratefully acknowledged.

References and Notes

(1) Karplus, M.; Weaver, D. L. *Biopolymers* **1979**, *18*, 1421.
(2) Karplus, M.; Weaver, D. L. *Nature (London)* **1976**, *260*, 404.
(3) Karplus, M.; Weaver, D. L. *Protein Sci.* **1994**, *3*, 650.
(4) Kim, P. S.; Baldwin, R. L. *Annu. Rev. Biochem.* **1982**, *51*, 459.
(5) Kim, P. S.; Baldwin, R. L. *Annu. Rev. Biochem.* **1990**, *59*, 631.
(6) Ballew, R. M.; Sabelko, J.; Gruebele, M. *PNAS* **1996**, *93*, 5759.
(7) Chowdhury, S.; Zhang, W.; Wu, C.; Xiong, G.; Duan, Y. *Biopolymers* **2003**, *68*, 63.
(8) Sung, S. S. *Biophys. J.* **1994**, *66*, 1796.
(9) Wu, X. W.; Sung, S. S. *Proteins* **1999**, *34*, 295.
(10) Wu, X.; Wang, S. *J. Phys. Chem. B* **2001**, *105*, 2227.
(11) Garcia, A. E.; Sanbonmatsu, K. Y. *Proc. Natl. Acad. Sci. U.S.A.* **2002**, *99*, 2782.
(12) Baldwin, R. L. *Proc. Natl. Acad. Sci. U.S.A.* **1986**, *83*, 8069.
(13) Lopez, M. M.; Chin, D. H.; Baldwin, R. L.; Makhatadze, G. I. *Proc. Natl. Acad. Sci. U.S.A.* **2002**, *99*, 1298.
(14) Padmanabhan, S.; York, E. J.; Stewart, J. M.; Baldwin, R. L. *J. Mol. Biol.* **1996**, *257*, 726.
(15) Scholtz, J. M.; Hong, Q.; York, E. J.; Stewart, J. M.; Baldwin, R. L. *Biopolymers* **1991**, *31*, 1463.
(16) Scholtz, J. M.; Marqusee, S.; Baldwin, R. L.; York, E. J.; Stewart, J. M.; Santoro, M.; Bolen, D. W. *Proc. Natl. Acad. Sci. U.S.A.* **1991**, *88*, 2854.
(17) Lockhart, D. J.; Kim, P. S. *Science* **1992**, *257*, 947.
(18) Lockhart, D. J.; Kim, P. S. *Science* **1993**, *260*, 198.
(19) Williams, S.; Causgrove, T. P.; Gilmanshin, R.; Fang, K. S.; Callender, R. H.; Woodruff, W. H.; Dyer, R. B. *Biochemistry* **1996**, *35*, 691.
(20) Thompson, P. A.; Eaton, W. A.; Hofrichter, J. *Biochemistry* **1997**, *36*, 9200.
(21) Lednev, I. K.; Karnoup, A. S.; Sparrow, M. C.; Asher, S. A. *J. Am. Chem. Soc* **1999**, *121*, 8074.
(22) Thompson, P.; Munoz, V.; Jas, G.; Henry, E.; Eaton, W.; Hofrichter, J. *J. Phys. Chem. B* **2000**, *104*, 378.
(23) Huang, C.; Klemke, J.; Getahun, Z.; DeGrado, W.; Gai, F. *J. Am. Chem. Soc.* **2001**, *123*, 9235.
(24) Case, D. A.; Pearlm, D. A.; Caldwell, J. W.; Cheatham, T. E., III; Wang, J.; Ross, W. S.; Simmerling, C.; Darden, T.; Merz, K. M.; Stanton, R. V.; Cheng, A.; Vincent, J. J.; Crowley, M.; Tsui, V.; Golhke, H.; Radmer, R.; Duan, Y.; Pitera, J.; Massova, I.; Seibel, G.; Singh, U. C.; Weiner, P.; Kollman, P. A. 2002.
(25) Duan, Y.; Chowdhury, S.; Xiong, G.; Wu, C.; Zhang, W.; Lee, T.; Cieplak, P.; Caldwell, J.; Luo, R.; Wang, J.; Kollman, P. A. *J. Comput. Chem.* **2003**, *24*, 1999.
(26) Bayly, C. I.; Cieplak, P.; Cornell, W. D.; Kollman, P. A. *J. Phys. Chem.* **1993**, *97*, 10269.
(27) Tsui, V.; Case, D. A. *J. Am. Chem. Soc.* **2000**, *122*, 2489.
(28) Berendsen, H. J. C.; Postma, J. P. M.; Vangunsteren, W. F.; Dinola, A.; Haak, J. R. *J. Chem. Phys.* **1984**, *81*, 3684.
(29) Ryckaert, J.-P.; Ciccotti, G.; Berendsen, H. J. C. *J. Comput. Phys.* **1977**, *23*, 327.
(30) Leopold, P. E.; Montal, M.; Onuchic, J. N. *Proc. Natl. Acad. Sci. U.S.A.* **1992**, *89*, 8721.
(31) Bryngelson, J. D.; Onuchic, J. N.; Socci, N. D.; Wolynes, P. G. *Proteins* **1995**, *21*, 167.
(32) Ferguson, N.; Fersht, A. R. *Curr. Opin. Struct. Biol.* **2003**, *13*, 75.
(33) Dill, K. A. *Biochemistry* **1990**, *29*, 7133.
(34) Avbelj, F.; Luo, P.; Baldwin, R. L. *Proc. Natl. Acad. Sci. U.S.A.* **2000**, *97*, 10786.
(35) Cui, B.; Shen, M. Y.; Freed, K. F. *Proc. Natl. Acad. Sci U.S.A.* **2003**, *100*, 7087.
(36) Hoffmann, D.; Knapp, E. *J. Phys. Chem. B* **1997**, *101*.
(37) Nymeyer, H.; Garcia, A. E. *PNAS* **2003**, *100*, 13934−13939.
(38) Wang, G.; Dunbrack, R. L., Jr. *Bioinformatics* **2003**, *19*, 1589.
(39) Pal, L.; Chakrabarti, P.; Basu, G. *J. Mol. Biol.* **2003**, *326*, 273.
(40) Baldwin, R. L. *Biophys. Chem.* **2002**, *101*, 203.
(41) Zagrovic, B.; Pande, V. *J. Comput. Chem.* **2003**, *24*, 1432.